Bull Volcanol (2008) 70:417–434
DOI 10.1007/s00445-007-0146-1

RESEARCH ARTICLE

Can crystallization of olivine tholeiite give rise to potassic rhyolites?—an experimental investigation

Matthew L. Whitaker · Hanna Nekvasil · Donald H. Lindsley · Michael McCurry

Received: 1 August 2005 / Accepted: 8 March 2007 / Published online: 20 June 2007
© Springer-Verlag 2007

Abstract Experiments were conducted to determine whether the rhyolites and basalts of the intraplate silica-saturated potassic suites could be genetically related through crystallization. Extreme crystallization (96–97%) of a high-MgO (10.62 wt%) olivine tholeiite from the Snake River Plain with an initial bulk water content of 0.4 wt% at a mid-crustal pressure of 4.3 kbar generated potassic rhyolitic liquids similar in major element chemistry to those found in the Quaternary rhyolite domes of the Snake River Plain and their plutonic equivalents in the Proterozoic Laramie Anorthosite Complex. Residual liquids comparable in composition to the bulk rock compositions of intermediate rocks found at the Craters of the Moon and Cedar Butte eruptive centers in the Snake River Plain are also generated along this crystallization path.

This paper constitutes part of a special issue dedicated to Bill Bonnichsen on the petrogenesis and volcanology of anorogenic rhyolites.

Editorial responsibility: E. Christiansen

M. L. Whitaker (✉) · H. Nekvasil · D. H. Lindsley
Department of Geosciences, Stony Brook University,
Stony Brook, NY 11794-2100, USA
e-mail: matthewlwhitaker@aim.com

H. Nekvasil
e-mail: hanna.nekvasil@sunysb.edu

D. H. Lindsley
e-mail: dlindsley@notes.cc.sunysb.edu

M. McCurry
Department of Geology, Idaho State University,
Pocatello, ID 83209, USA
e-mail: mccumich@isu.edu

Keywords Crystallization · Differentiation · Potassic rhyolites · Experimental · Snake River Plain · Tholeiite · Basalt

Introduction

Rhyolites and granites of continental intraplate magmatic regimes are commonly spatially and temporally associated with a variety of mafic and intermediate rocks that share specific compositional characteristics. These shared characteristics have provided the foundation for systematizing the diversity of intra-plate magmatic rock associations into several series (Nekvasil 1998; Nekvasil et al. 2000, 2003). Characteristic of the silica-saturated potassic series (i.e., the continental tholeiitic series of Nekvasil et al. 2000) is the presence of potassic rhyolite/granite in addition to tholeiitic basalt/gabbro. Volcanic suites in this series include those of the hotspot-related large igneous provinces (e.g., Yellowstone–Snake River Plain volcanic province) which form the sequence tholeiitic basalt–ferrobasalt–trachybasalt–trachyandesite–trachyte (tristanite)–potassic rhyolite (Frost and Frost 1997; Leeman et al. 1976; McCurry et al. 1999, this issue; Stout et al. 1994), or, more commonly, bimodal basalt/potassic rhyolite associations. Plutonic suites within this series consist of the non-cumulate rocks of the massif anorthosite complexes (Frost et al. 1993, 1999; Scoates et al. 1996) which follow the sequence olivine gabbro–ferrodiorite (jotunite)–monzodiorite–monzonite–monzosyenite–syenite–potassic granite (Fig. 1).

Figure 1 shows the characteristic variation in total alkalis vs silica in rocks of the silica-saturated potassic series,

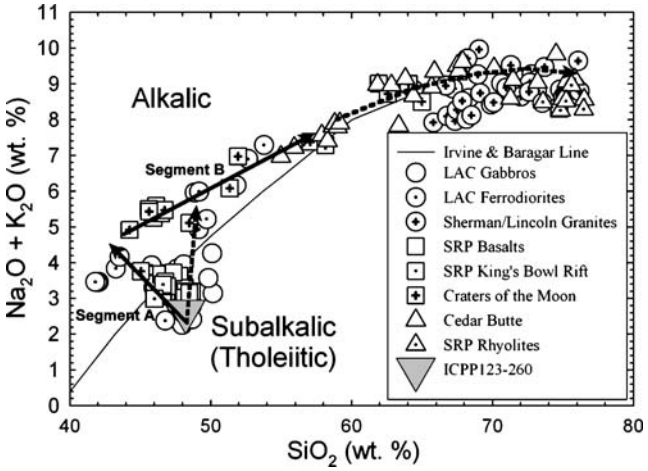

Fig. 1 Total alkalis vs silica variation in bulk compositions of natural rocks of the silica-saturated potassic trend from the Snake River Plain (SRP basalts, basalts of the SRP King's Bowl rift, basalts and intermediate rocks of Craters of the Moon lava field, intermediate rocks and rhyolites of Cedar Butte, and SRP rhyolites) and fine-grained rocks of the Laramie Anorthosite Complex (LAC Gabbros, LAC Ferrodiorites, and Sherman/Lincoln Granites). All data presented are normalized to 100% on a volatile-free basis. Data from Mitchell et al. (1995, 1996), Frost et al. (1999), Kuntz et al. (1992), Stout and Nicholls (1977), Leeman et al. (1976), Stout et al. (1994), McCurry et al. (this issue), and Leeman (1982). The Irvine and Baragar line separates the alkalic and subalkalic fields (Irvine and Baragar 1971). The silica-depletion trend is shown by the solid line segment A; the silica enrichment path is shown by the solid line segment B. *Dashed arrows* indicate possible additional trends. ICPP123-260 is the olivine tholeiite used as the parent material in this study

exemplified by rocks from the Snake River Plain and Laramie Anorthosite Complex. This potassic series differs distinctly from the silica-saturated sodic alkalic series of Nekvasil et al. (2004; e.g., lavas of Ascension Island and the Nandewar Volcano of Australia) which is characterized by the more strongly alkalic character of the intermediate rocks and higher Na_2O/K_2O ratios of rhyolites and granites.

The silica-saturated potassic trend can be subdivided into two primary segments; one trending toward silica-depletion and the other toward silica-enrichment. The silica-depletion trend emanates from the least evolved tholeiitic/gabbroic rocks and extends toward low-silica, high Fe–Ti–P ferrobasaltic (ferrodioritic/jotunitic) rocks (Fig. 2), crossing the subalkalic–alkalic boundary on a total alkalis vs silica diagram (segment A, Fig. 1). The silica-enrichment segment of the trend emanates from the ferrobasalts and extends through the trachybasalt and trachyandesite fields (segment B, Fig. 1). A possible bridging trend between tholeiitic basalts and trachyandesites is indicated by a dashed arrow, as is the possible evolutionary path to trachytes and potassic rhyolites.

The possibility of a genetic relationship between tholeiites and the low silica, Fe–Ti–P–rich rocks of this trend (segment A, Fig. 1) has been verified experimentally. Thompson (1975), Litvin (2002) and Whitaker et al. (2003) have determined experimentally that the silica-depletion, Fe–Ti–P–enrichment trend leading to the ferrobasalts of the volcanic suites can be reproduced by crystallization of a tholeiitic parent melt at lower crustal pressures (9.3 kbar) under nominally anhydrous (~0.05 wt% H_2O) conditions. Similarly, Scoates et al. (1999) determined experimentally that the ferrodiorites (jotunites) of the anorthosite complexes can be generated by differentiation of high-aluminum olivine gabbroic liquids under the same conditions of crystallization.

Generation of liquids falling along segment B of the silica-saturated potassic trend by continued crystallization of tholeiite-derived ferrobasaltic liquids has been suggested previously. Scoates et al. (1996) suggested that the ferrodiorites of the anorthosite complexes may be able to generate monzonitic liquids by crystallization. Similarly, experimental and analytical work by Leeman et al. (1976), and analytical work by Stout et al. (1994) suggested that the more evolved trachyandesitic rocks of the Craters of the Moon (COM) suite in the Snake River Plain could be generated primarily by crystallization of a ferrobasaltic liquid in the lower crust. However, the nature of the relationship between the mafic and intermediate rocks and the most silicic rocks (trachytes, potassic rhyolites and granites) of this series remains unclear.

Several workers have hypothesized that the mafic and intermediate magmas only provide the heat needed for partial melting of crustal material in the silica-saturated potassic suites and are not co-magmatic with the associated felsic rocks (e.g., Anderson 1983; Haapala and Ramo 1990). This hypothesis was supported by the observation of less voluminous material of mafic and intermediate composition than would be expected if crystallization or partial melting of this material were the primary process producing potassic rhyolites and granites. However, several chemical characteristics, such as low fO_2, high Fe/Mg, and the potassic nature of the rhyolitic rocks, suggest that these rocks may be more closely related than by heat transfer alone (Frost et al. 1999). Furthermore, if crystallization or partial melting had taken place at depth, volumetric relations exposed at shallower levels need not be significant. Other workers have instead suggested the potassic granites and rhyolites may be generated either by partial melting (e.g. Frost and Frost 1997, 1999) or crystallization (e.g. Hunter and Sparks 1987; McCurry et al. this issue; Rossier et al. 2001) of the mafic and/or intermediate rocks. To date, no definitive experimental data to verify such possibilities have been reported.

This paper presents new data arising from the experimental investigation of the possibility that the silicic rocks of the silica-saturated potassic series lie on the liquid line-of descent of crystallizing tholeiitic magma. Two suites within this series are accorded specific attention, the volcanic suite of Cedar Butte of the Snake River Plain and the plutonic

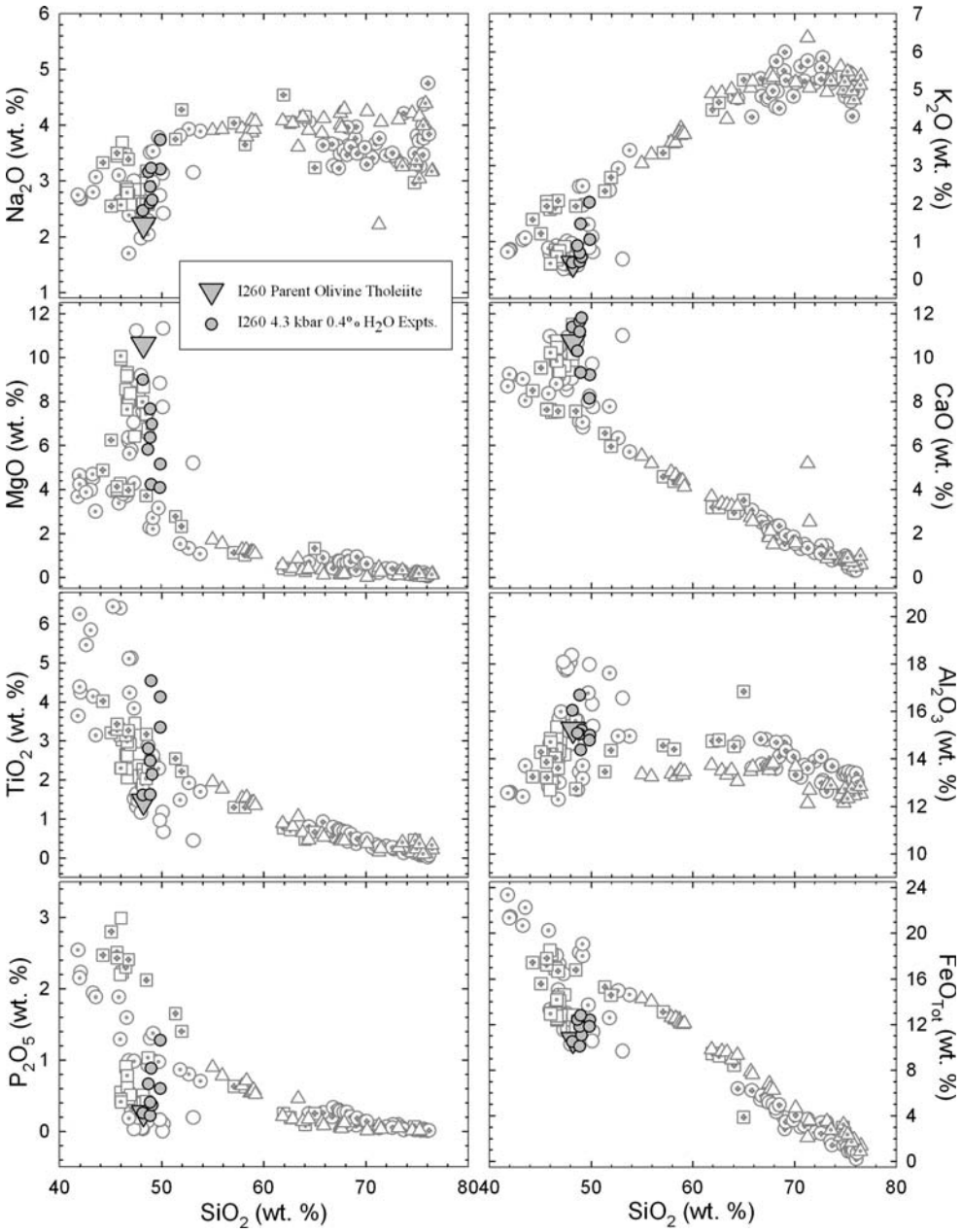

Fig. 2 Major element variation of bulk compositions of non-cumulate rocks from the LAC and SRP suites. Samples and sources are as in Fig. 1. Experimental residual liquid compositions of experiments on I260 olivine tholeiite (*gray triangle*) at 4.3 kbar and 0.4 wt% bulk water content (*gray circles*) are shown

suite of the Laramie Anorthosite Complex, in order to enable direct comparison of experimental liquids with natural rocks.

Geologic background

Snake River Plain As exposed, volcanics of the Snake River Plain are dominantly bimodal basalt/rhyolite associations, but there are at least two eruptive centers where intermediate rocks can be found: the Craters of the Moon volcanic field, and the Cedar Butte volcanic center. Craters of the Moon rocks range in composition from basalts and ferrobasalts to trachyandesites; Cedar Butte contains rocks that range in composition from trachyandesite to potassic rhyolite. With few exceptions, these are all crystal-poor volcanic rocks that closely resemble liquid compositions. The most evolved rocks of the Craters of the Moon suite and the least evolved rocks from Cedar Butte overlap in major element composition (Figs. 1, 2 and 3).

Trace-element concentrations of the intermediate to rhyolitic rock series found at Cedar Butte vary systematically with major-element bulk composition, defining linear to strongly curvilinear co-variation trends. In the latter case, changes in slopes of the trends correlate closely with observed changes in phenocryst assemblages and composition (McCurry et al. this issue). Sr- and εNd-isotopic analyses of intermediate to low-silica rhyolites overlap with

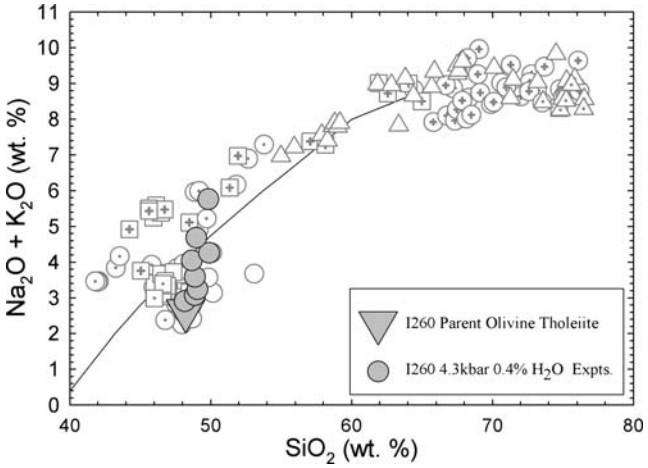

Fig. 3 Total alkalis vs silica variation of residual liquid compositions of experiments on I260 olivine tholeiite (*gray triangle*) at 4.3 kbar and 0.4 wt% bulk water content (*gray circles*). Other symbols are as in Fig. 1

those of temporally related olivine tholeiite (~0.7065 to 0.707 and ~−3 to −6, respectively), and differ strongly from the highly isotopically evolved Archean crustal rocks. The most evolved high-silica rhyolites (~75–76% SiO_2) are similar in εNd, but have slightly more evolved $^{87}Sr/^{86}Sr_i$ (~0.708 to 0.7097), suggesting only very minor crustal assimilation. However, since these rhyolites have very low bulk Sr (~1 ppm), the Archean crustal component is limited to less than ~1%. Based on such isotopic and trace element considerations, McCurry et al. (this issue) suggest that the Quaternary rhyolites of the Snake River Plain are related by crystallization to the less evolved intermediate rocks typical of the Craters of the Moon and Cedar Butte suites.

It should be noted here that the Quaternary potassic rhyolites discussed in this paper differ from the voluminous ignimbrites found in the region. The ignimbrites are higher in MgO, TiO_2, CaO, and total alkalis and lower in FeO/MgO ratio compared to the Quaternary rhyolites of the Snake River Plain (Christiansen and McCurry, this issue), and thus do not fall along the same compositional trends as rocks discussed in this work.

Detailed comparison of experimental results with natural bulk rock compositions will focus on the rocks of Cedar Butte because of their small degree of crustal contamination. However, even though it is generally accepted that Craters of the Moon rocks do exhibit varying degrees (1–15%) of crustal contamination (Leeman 1982a, b; Leeman et al. 1976; Stout et al. 1994; Thompson 1975), the similarity in major element compositions of rocks of these two suites suggests that contamination has not obscured any primary differentiation trends.

Laramie Anorthosite Complex The most voluminous plutons found exposed in the Laramie Anorthosite Complex consist of anorthosite and potassic granite with smaller bodies of mafic and intermediate compositions located around the margins of, or intruding into, these larger stocks and batholiths. The non-cumulate units are similar to the lavas of the Snake River Plain suites, but with more extreme Fe–Ti–P-enrichment in the plutonic suites. The potassic granites found associated with the Laramie Anorthosite Complex bear a strong compositional resemblance to potassic "anorogenic" granite batholiths such as the Wolf River batholith, the main body of the Pikes Peak batholith (e.g., Emslie 1978; Emslie 1991; Frost and Frost 1997), and the wiborgite of the Fennoscandian regions (e.g., Vorma 1976). All of these are markedly similar in bulk chemical composition to the Quaternary potassic rhyolites of the Snake River Plain, suggesting that they may represent liquid compositions. The compositional similarity between the granites of these intrusive complexes and the Quaternary rhyolitic lavas of the Snake River Plain suggests that these magmas may have formed as a result of similar processes and perhaps from similar parent magma compositions.

Experimental strategy

The experiments conducted for this study focused on determining the liquid-line-of descent and mineral assemblages of a tholeiite as it ponds and undergoes equilibrium crystallization within the crust, producing liquids which eventually separate, rise toward the surface, and are either emplaced at shallower levels or erupt at the surface. Removal of liquid once 80% crystallinity had been

Table 1 Compositions of Experimental Starting Materials (wt%)

Starting Material (no.) Rock type	ICPP123-260 (I260) Natural olivine tholeiite	100D3 Synthetic trachybasalt glass
SiO_2	47.53	47.91
TiO_2	1.43	4.06
Al_2O_3	15.03	14.06
FeO_{Tot}	10.53	12.94
MnO	0.16	0.22
MgO	10.46	3.89
CaO	10.57	8.69
Na_2O	2.18	2.93
K_2O	0.42	1.53
P_2O_5	0.26	1.02
Total	98.58	97.25
Mg#[a]	0.68	0.39
H_2O in Glass (wt%)[b]	0.4	1.8

[a] Mg#=molar Mg/(Mg+Fe^{2+}) assuming an Fe^{2+}/Fe_{Tot} ratio of 0.85
[b] Measured by FTIR

Table 2 Representative residual liquid compositions of I260 experiments with 0.4 bulk wt% H_2O[a] at 4.3 kbar

Experiment (no.)	I260-133	I260-96	I260-127	I260-125
Mode (wt%)	Gl 95.3%, Ol 4.7%	Gl 91.6%, Ol 8.4%	Gl 73.2%, Ol 13.0%, Pl 12.9%, Cpx 0.9%	Gl 57.9%, Ol 15.4%, Pl 20.2%, Cpx 6.5%
Temperature (°C)	1,220	1,200	1,180	1,160
SiO_2	47.02	47.68	48.05	47.17
TiO_2	1.57	1.59	2.09	2.40
Al_2O_3	15.66	16.28	14.89	14.51
FeO	10.25	9.84	10.80	11.41
MnO	0.16	0.14	0.20	0.25
MgO	8.78	7.48	6.83	6.15
CaO	11.11	11.34	11.56	10.78
Na_2O	2.41	2.54	2.60	2.79
K_2O	0.44	0.46	0.58	0.67
P_2O_5	0.25	0.21	0.36	0.39
Total	97.64	97.56	97.95	96.52
Mg#	0.64	0.61	0.57	0.53
H_2O in Glass (wt%)[b]	0.4	0.4	0.5	0.6
Crystallinity (wt%)	4.7	8.4	26.8	42.1
S.S.R.	0.08	0.04	0.06	0.06
Experiment (no.)	I260-90	I260-120	I260-100	I260-97
Mode (wt%)	Gl 43.4%, Ol 17.0%, Pl 27.1%, Cpx 12.5%	Gl 35.2%, Ol 18.5%, Pl 30.0%, Cpx 16.3%	Gl 19.8%, Ol 21.9%, Pl 40.1%, Cpx 18.2%	Gl 15.3%, Ol 21.9%, Pl 41.6%, Cpx 21.0%, Ilm 0.2%
Temperature (°C)	1,140	1,120	1,100	1,080
SiO_2	46.39	47.30	47.73	46.95
TiO_2	2.67	3.17	4.42	3.89
Al_2O_3	14.38	14.21	14.01	13.93
FeO	11.83	11.76	12.44	11.14
MnO	0.21	0.16	0.21	0.17
MgO	5.55	4.88	4.12	3.84
CaO	9.81	8.73	9.08	7.66
Na_2O	3.01	3.04	3.15	3.52
K_2O	0.85	1.00	1.42	1.91
P_2O_5	0.63	0.56	0.86	1.20
Total	95.32	94.81	97.43	94.20
Mg#	0.50	0.47	0.41	0.42
H_2O in glass (wt%)[b]	0.8	1.0	1.8	2.3
Crystallinity (wt%)	56.6	64.8	80.2	84.7
S.S.R.[c]	0.13	0.05	0.03	0.14

[a] Measured by FTIR
[b] Calculated based on bulk water content and degree of crystallinity
[c] S.S.R. Sum of squared residuals

achieved was simulated for these experiments by synthesizing a new bulk composition that matched the composition of the residual liquid. Crystallization of this new liquid composition allowed for more detailed evaluation of the last stages of crystallization.

Crystallization experiments were conducted at pressures ranging from 9.3 kbar to "0" kbar (DiFrancesco et al. 2003; Whitaker et al. 2003, 2004). However, only experimental results at 4.3 kbar are reported here since they produced a spectrum of liquids similar to the intermediate rocks and potassic rhyolites of this series. Potassic rhyolitic glass was not produced at 9.3 or 6.8 kbar at any water content investigated (Whitaker et al. 2003; personal communication); sodic rhyolite similar to that of ocean islands such as the Galapagos was produced below about 2.5 kbar by Spulber and Rutherford (1983) from a Kilauea basalt, and at "0" kbar from the same olivine tholeiite used in the experiments reported here by DiFrancesco et al. (2003). Therefore, the experimental data reported in this paper are of relevance for pressures below 6.8 kbar and above 2.5 kbar.

Experimental methods

Starting materials

The starting material for most experiments was a natural olivine tholeiite from the eastern Snake River Plain (ICPP123-260, abbreviated hereafter as I260; see Table 1), selected for its high Mg#, high MgO content, low Ni content, paucity of phenocrysts, and freshness. It is a mildly vesicular rock that contains ~2 vol.% phenocrystic olivine and lesser amounts of plagioclase phenocrysts. The groundmass of the rock is composed primarily of plagioclase, clinopyroxene, and olivine, with minor amounts of Fe–Ti oxides, quenched glass, olivine altered to iddingsite, and trace amounts of apatite. The compositions of olivine phenocrysts and groundmass olivines are similar. When combined with the low bulk Ni content, this suggests that the high Mg content of I260 does not result from accumulated olivine and that I260 could represent a liquid.

Experiments below 1100°C were conducted using a synthetic mix (100D3; Table 1) that matched the composition of the residual trachybasaltic liquid produced during equilibrium crystallization at 1,100°C. This liquid composition was selected because it was produced at the lowest temperature crystallization experiment on I260 that yielded liquids that could still be analyzed with confidence; lower temperature experiments on I260 yielded isolated glass patches with heterogeneous compositions once the crystallinity exceeded 80 wt%. Use of this synthetic composition permitted assessment of liquid evolution at lower temperatures closer to that of the solidus.

Table 3 Representative mineral compositions of I260 experiments with 0.4 bulk wt% H_2O at 4.3 kbar

Phase	Olivine						
Experiment (no.)	I260-133	I260-96	I260-127	I260-125	I260-90	I260-120	I260-100
Temperature (°C)	1,220	1,200	1,180	1,160	1,140	1,120	1,100
SiO_2	39.56	39.14	38.40	38.30	36.73	36.96	37.42
TiO_2	0.00	0.02	0.05	0.08	0.07	0.11	0.04
Al_2O_3	0.08	0.07	0.07	0.06	0.07	0.06	0.03
FeO	15.31	16.81	18.70	20.98	24.47	25.77	28.20
MnO	0.17	0.20	0.23	0.32	0.29	0.31	0.36
MgO	44.05	42.04	40.73	37.85	35.17	34.83	31.95
CaO	0.34	0.32	0.36	0.42	0.40	0.42	0.36
Na_2O	0.03	0.00	0.01	0.01	0.00	0.00	0.02
K_2O	0.01	0.01	0.00	0.00	0.01	0.00	0.01
P_2O_5	0.14	0.01	0.07	0.02	0.02	0.06	0.05
Total	99.68	98.60	98.63	98.02	97.24	98.53	98.43
Phase comp. (mol%)	Fo83(La0.5)	Fo81(La0.5)	Fo79(La0.5)	Fo76(La0.5)	Fo72(La0.5)	Fo70(La0.6)	Fo67(La0.6)
Phase	Olivine	Plagioclase					
Experiment (no.)	I260-97	I260-127	I260-125	I260-90	I260-120	I260-100	I260-97
Temperature (°C)	1,080	1,180	1,160	1,140	1,120	1,100	1,080
SiO_2	35.46	50.20	50.48	49.96	50.93	52.26	50.71
TiO_2	0.12	0.05	0.09	0.08	0.14	0.28	0.31
Al_2O_3	0.08	30.91	30.48	30.27	30.00	29.19	28.27
FeO	29.82	0.30	0.45	0.67	0.74	1.06	0.88
MnO	0.41	0.00	0.01	0.03	0.00	0.01	0.03
MgO	30.71	0.20	0.24	0.24	0.31	0.33	0.31
CaO	0.38	14.14	14.14	13.63	13.33	12.90	12.35
Na_2O	0.02	3.21	3.23	3.32	3.47	3.91	4.01
K_2O	0.01	0.16	0.17	0.17	0.21	0.30	0.33
P_2O_5	0.11	0.03	0.07	0.23	0.04	0.08	0.23
Total	97.12	99.20	99.35	98.59	99.18	100.32	97.43
Phase comp. (mol%)	Fo64(La0.6)	An70(Or1)	An70(Or1)	An69(Or1)	An67(Or1)	An63(Or2)	An62(Or2)
Phase	Augite						Ilmenite
Experiment (no.)	I260-127	I260-125	I260-90	I260-120	I260-100	I260-97	I260-97
Temperature (°C)	1,180	1,160	1,140	1,120	1,100	1,080	1,080
SiO_2	50.03	49.09	48.48	48.06	49.41	47.81	0.11
TiO_2	0.98	1.38	1.33	2.35	1.87	2.19	52.29
Al_2O_3	5.29	5.71	4.38	5.74	4.35	4.68	0.44
FeO	5.26	6.35	6.98	7.23	8.36	8.37	37.15
MnO	0.12	0.15	0.17	0.19	0.18	0.23	0.50
MgO	14.39	14.15	14.36	13.14	13.59	13.15	6.29
CaO	21.16	20.19	19.84	20.00	20.07	19.57	0.30
Na_2O	0.30	0.32	0.31	0.35	0.40	0.40	0.02
K_2O	0.00	0.00	0.01	0.01	0.01	0.02	0.01
P_2O_5	0.03	0.07	0.30	0.05	0.06	0.35	0.01
Total	97.54	97.40	96.15	97.12	98.29	96.77	98.13
Phase comp. (mol%)	En51Wo39	En50Wo37	En49Wo39	En47Wo39	En45Wo39	En45Wo39	Ilm97Hem3

Sample preparation

I260 was prepared for experiments by crushing in an agate shatterbox and grinding in an agate mortar, resulting in a fine powder with an average grain size of several microns. This powder was loaded into a graphite capsule and the lid inserted. The loaded capsule was dried for one hour under vacuum at 150°C to drive off any adsorbed water while retaining the structurally bound water. Once dried, the capsule was immediately placed into the cell assembly in the piston-cylinder apparatus and pressurized to a few kbar in order to prevent re-adsorption of water. The bulk water content of a fused sample prepared in this way was determined by micro-Fourier transform infrared spectroscopy (FTIR) to be 0.4 wt%.

The derivative composition, 100D3, was synthesized from a mixture of high-purity gels and oxides that was homogenized in an agate mortar. A Fe^{2+}/Fe_T ratio of 0.85

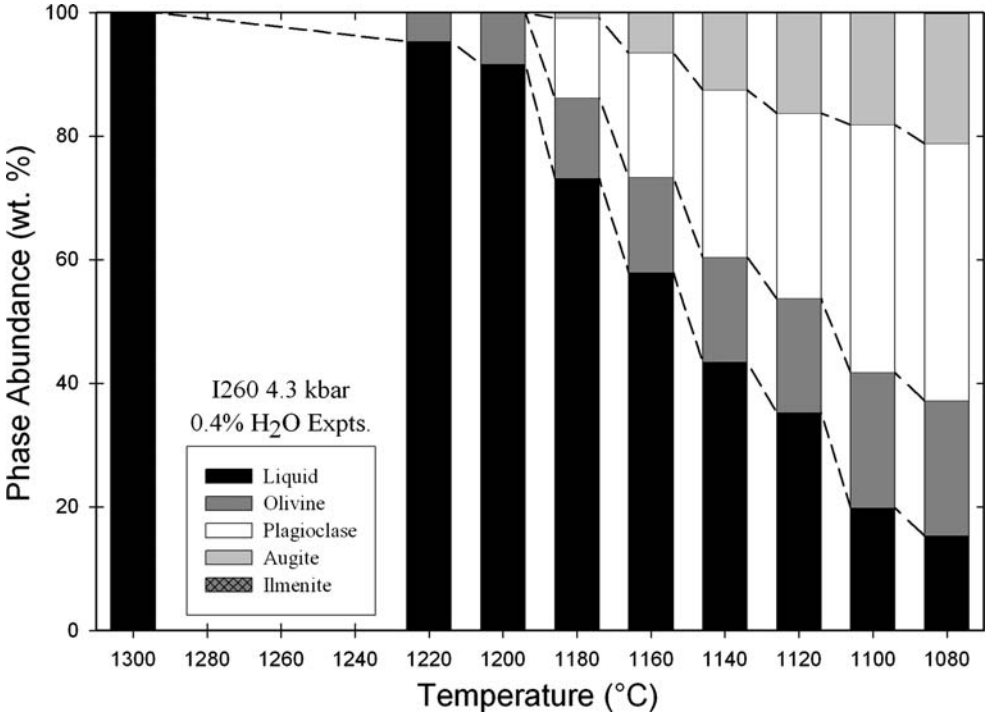

Fig. 4 Variation in phase abundances with temperature of experimental run products of I260 at 4.3 kbar and 0.4 wt% bulk water content

for the mix was achieved by weighing. The addition of water to the mix required an additional step because graphite is porous to structurally unbound water. A hydrous glass containing 8.5 wt% H_2O (as determined by FTIR) was made in a large-volume, graphite-lined Pt capsule at 10 kbar (nominal). The hydrous glass was crushed and mixed with the non-hydrated starting material (which has 1 wt% H_2O as determined by FTIR) in the requisite amounts to yield a bulk water content of 1.8 wt%. This is the water content of the residual glass of the 1,100°C experiment on I260 (the composition emulated by 100D3). The graphite capsule imposed a fO_2 on the system which kept the Fe^{2+}/Fe_T ratio between 0.85 and 0.90 (as determined by micro-XANES). The final composition of the mix was checked for accuracy by melting at 4.3 kbar in graphite, quenching to a glass, and analyzing by electron microprobe and micro-FTIR.

Experimental procedure

All experiments were carried out in an end-loaded solid medium piston-cylinder apparatus using a cell assembly consisting of a $BaCO_3$ outer sleeve, graphite furnace, and dried mullite and crushable MgO spacers (which held the graphite capsule centered with respect to the hotspot of the assembly). The graphite capsule was in direct contact with the graphite furnace, thereby effectively becoming part of the furnace assembly. An insulating alumina disc prevented the

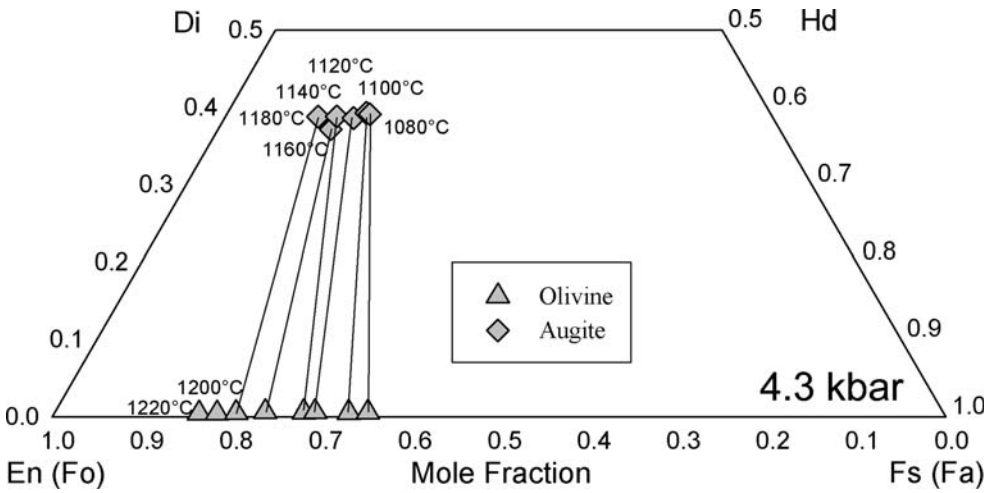

Fig. 5 QUILF projections of olivine and pyroxene compositions from experimental run products of I260 at 4.3 kbar and 0.4 wt% bulk water content. Tie-lines connect coexisting phases. Temperatures of experiments are indicated

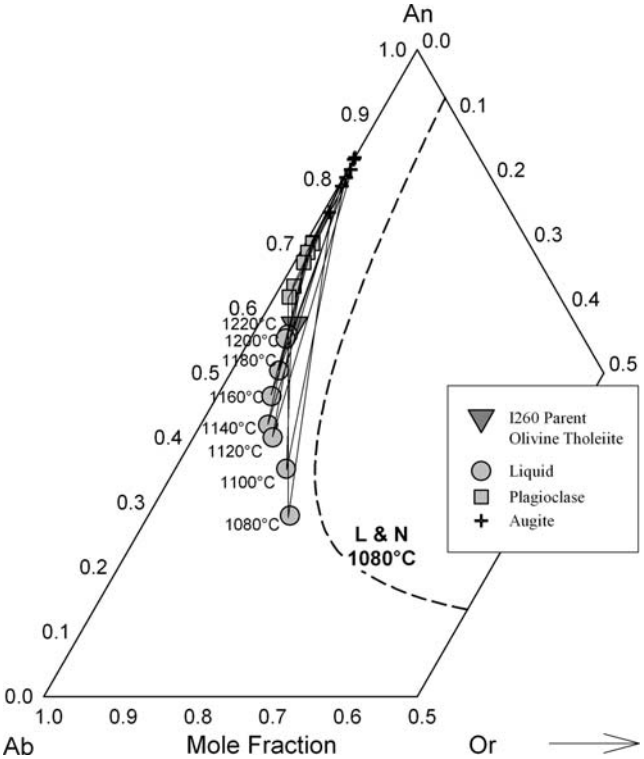

Fig. 6 Plagioclase compositions (*gray squares*) and molar normative feldspar constituents of glass (*gray circles*) and pyroxene (*black crosses*) of I260 experiments at 4.3 kbar and 0.4 wt% bulk water content. Tie-lines connect coexisting phases. Temperatures of these experiments are indicated. The isothermal ternary feldspar solvus section computed using the model of Lindsley and Nekvasil (1989) and the software of Wen and Nekvasil (1994) for 1,080°C and 4.3 kbar is shown by the *dashed curve*

thermocouple from contacting the graphite. Temperature was monitored and controlled with a Pt–$Pt_{90}Rh_{10}$ thermocouple. Temperature calibration yielded a temperature gradient of +14°C from the thermocouple to the center of the capsule; the temperatures reported here are those at the hotspot of the sample. The pressure calibration of this cell assembly using the subsolidus reaction Mg−cordierite= Sapphirine+Quartz (Newton et al. 1974) at 7 kbar yielded a −0.7 kbar correction factor; all reported pressures have been corrected.

The experiments reported were crystallization experiments conducted using the piston-out method. The cell assembly was slowly brought up to a pressure ~2 kbar greater than the desired pressure at room temperature. The sample was then heated to the melting temperature (1,300°C), after which the pressure was decreased to 4.3 kbar. The sample remained at the melting temperature for 2 h to ensure complete fusion. After fusion, the temperature was rapidly dropped to the final crystallization temperature of the experiment, where the sample remained for 2–3 days. At the conclusion of each experiment, the run products were quenched by turning off the power (resulting in an initial cooling rate of ~100°C/s).

Analytical techniques

The major element compositions of all phases in the experimental run products were analyzed by electron microprobe. All olivine, pyroxene, and oxide analyses were projected through QUILF (Andersen et al. 1993) in order to check for Fe:Mg exchange equilibrium and to compute fO_2 when the phase assemblage permitted. The fO_2 was computed to be ~1.8–2.6 log units below FMQ in the experiments.

The IgPet Program Suite (Carr 2002) was used to calculate molar norms of all liquids and pyroxenes for projection into the feldspar system and to conduct mass balance calculations using a least squares routine. The mass balance calculations yielded estimates of phase proportions and helped ensure that no phases were overlooked. Only those phase combinations which yielded sums of the squares of the residuals less than 0.15 are reported in this work.

The water contents of selected experimental glasses were measured by micro-IR spectroscopy using the Nicolet 20SXB FTIR spectrometer and Spectra Tech IR Plan microscope at the American Museum of Natural History. Glass densities and total water concentrations were calculated via the methods in Dixon et al. (1995) and Mandeville et al. (2002).

Experimental results

The run products of each experiment contained variable amounts of crystalline phases and residual glass. Mineral zoning was rarely observed except in clinopyroxene, which often exhibited significant variation in non-quadrilateral components, particularly Al and Ti. Water was retained within quenched glass for all experiments until vapor-phase saturation was attained. With decreasing temperature below this point, dissolved water contents remained relatively constant as the amount of glass decreased. Fluid may have been lost through the graphite capsule wall; however, mass balance calculations revealed that no notable change in bulk chemistry accompanied any possible fluid loss.

I260 experiments

All experiments conducted for this study using the I260 olivine tholeiite parent material were carried out at 4.3 kbar with a bulk water content of 0.4 wt% H_2O. Tables 2 and 3 give representative experimental residual liquid and mineral compositions. Figures 2 and 3 show chemical evolution of the residual liquid during equilibrium crystallization from the olivine tholeiite parent composition to trachybasaltic liquids. As crystallization progresses with falling temperature, there is an increase in total alkalis while silica remains

fairly constant, indicating that tholeiitic basalt can differentiate to form mildly alkalic silica-saturated liquids at mid-crustal pressures (Fig. 3).

For this composition, olivine is the liquidus phase and persists throughout the range of explored temperatures. Augite and plagioclase follow; within the 20°C interval of these experiments, they join the assemblage simultaneously. Plagioclase becomes volumetrically dominant shortly after it enters the assemblage, and remains so throughout the range of temperatures investigated. Augite never surpasses olivine in abundance. In the lowest temperature experiment, ilmenite joins the crystallizing assemblage (Fig. 4).

Figure 5 shows olivine and pyroxene compositions as projected through QUILF (Andersen et al. 1993) via the method of Lindsley and Andersen (1983). The forsterite component of the olivines decreases from Fo_{83} in the highest temperature experiment to Fo_{64} in the lowest, while the enstatite component of the augites decreases from En_{51} to En_{45} at nearly constant Wo ($Wo_{37–39}$).

The relationships between the liquids, feldspars, and pyroxenes in feldspar compositional space are shown in Fig. 6. The molar normative feldspar constituents of the residual liquids and pyroxenes were calculated and renormalized to 1. The ternary components of the feldspar crystals were obtained directly from the atomic ratios given by the microprobe and also renormalized. The anorthite component in the plagioclase decreased from An_{70} to An_{62} with decreasing temperature, while the orthoclase component increased very little, from $Or_{<1}$ to Or_2. Crystallization of augite and anorthitic plagioclase drives the liquid away from the An apex toward increasing Ab and Or. With falling temperature, crystallization of more intermediate plagioclase causes the liquid to evolve toward more Or-rich compositions.

100D3 derivative liquid experiments

Along this portion of the crystallization path, the liquids evolve from the 100D3 trachybasaltic parent composition through trachyandesite and trachyte, eventually producing potassic rhyolitic liquids. Tables 4 and 5 list representative experimental residual liquid and mineral compositions along this path; Figs. 7 and 8 show the compositional evolution of the residual liquids.

Olivine, augite, plagioclase, and ilmenite are present in the assemblage of the highest temperature experiment and persist throughout the range of temperatures explored. Augite dominates early, but is quickly replaced by plagioclase as the volumetrically dominant mineral phase in the assemblage. Apatite is the next mineral to crystallize, and is present throughout the remainder of the experimental temperature range. In the lowest temperature experiment

Table 4 Representative residual liquid compositions of 100D3 experiments with 1.8 bulk wt% H_2O[a] at 4.3 kbar

Experiment (no.)	100D3-04	100D3-03	100D3-06	100D3-07	100D3-09
Mode (wt%)	Gl 78.8%, Ol 0.7%, Pl 3.2%, Cpx 13.9%, Ilm 3.4%	Gl 37.1%, Ol 9.2%, Pl 26.4%, Cpx 19.4%, Ilm 5.9%, Ap 2.0%	Gl 30.3%, Ol 11.6%, Pl 30.2%, Cpx 19.8%, Ilm 6.4%, Ap 1.7%	Gl 20.0%, Ol 9.8%, Pl 39.6%, Cpx 21.6%, Ilm 6.9%, Ap 2.1%	Gl 14.4%, Ol 5.7%, Pl 44.0%, Cpx 23.5%, Ilm 7.5%, Ap 2.2%, Pig 2.7%
Temperature (°C)	1,040	1,000	980	960	940
SiO_2	49.02	58.25	63.97	65.47	68.12
TiO_2	2.32	1.04	0.87	0.61	0.57
Al_2O_3	15.09	15.18	15.12	14.79	14.51
FeO	12.20	7.96	5.72	4.28	3.41
MnO	0.27	0.18	0.09	0.09	0.03
MgO	2.50	0.99	0.59	0.42	0.28
CaO	6.94	3.96	2.67	2.17	1.57
Na_2O	3.28	3.93	4.01	3.94	3.74
K_2O	1.83	4.10	5.07	5.48	5.96
P_2O_5	1.08	0.55	0.41	0.26	0.21
Total	94.53	96.14	98.54	97.51	98.40
Mg#	0.30	0.21	0.18	0.17	0.15
H_2O in Glass (wt%)	2.2[b]	<4.7[c]	<5.8[c]	?[d]	?[d]
Crystallinity (wt%)	21.1	62.9	69.7	80.0	85.6
S.S.R.[e]	0.02	0.10	0.08	0.03	0.08

[a] Measured by FTIR
[b] Calculated based on bulk water content and degree of crystallinity
[c] Estimation required because of the small size of the glass patches and presence of apatite
[d] Loss of a fluid phase likely
[e] S.S.R. Sum of squared residuals

Table 5 Representative mineral compositions of 100D3 experiments with 1.8 wt% H_2O at 4.3 kbar

Phase	Olivine					Plagioclase	
Experiment (No.)	100D3-04	100D3-03	100D3-06	100D3-07	100D3-09	100D3-04	100D3-03
Temperature (°C)	1,040	1,000	980	960	940	1,040	1,000
SiO_2	35.14	32.87	32.85	32.47	32.22	54.74	54.73
TiO_2	0.09	0.15	0.14	0.14	0.34	0.12	0.10
Al_2O_3	0.05	0.06	0.05	0.07	0.09	28.33	27.91
FeO	38.30	48.00	50.41	51.90	53.31	0.57	0.49
MnO	0.54	0.76	0.86	0.84	0.82	0.00	0.02
MgO	25.37	17.13	14.75	14.18	13.23	0.07	0.07
CaO	0.35	0.33	0.43	0.39	0.47	11.24	10.89
Na_2O	0.00	0.02	0.00	0.02	0.03	4.81	4.93
K_2O	0.01	0.01	0.03	0.00	0.07	0.53	0.46
P_2O_5	0.07	0.21	0.18	0.21	0.15	0.26	0.07
Total	99.91	99.54	99.70	100.21	100.74	100.67	99.66
Phase comp. (mol%)	Fo54(La0.5)	Fo39(La0.5)	Fo34(La0.7)	Fo32(La0.7)	Fo30(La0.8)	An55(Or3)	An54(Or3)
Phase	Plagioclase			Augite			
Experiment (No.)	100D3-06	100D3-07	100D3-09	100D3-04	100D3-03	100D3-06	100D3-07
Temperature (°C)	980	960	940	1,040	1,000	980	960
SiO_2	55.15	56.01	56.53	46.42	45.26	46.05	48.84
TiO_2	0.14	0.41	0.09	3.02	3.59	2.44	1.47
Al_2O_3	28.05	26.89	27.12	7.18	6.85	7.80	3.24
FeO	0.59	0.74	0.74	10.50	14.95	13.42	18.31
MnO	0.00	0.03	0.00	0.29	0.32	0.32	0.45
MgO	0.10	0.06	0.05	11.25	10.28	9.51	10.76
CaO	10.58	9.76	9.49	19.98	16.67	20.00	15.49
Na_2O	5.06	5.40	5.56	0.45	0.39	0.31	0.26
K_2O	0.49	0.72	1.11	0.02	0.04	0.03	0.04
P_2O_5	0.22	0.21	0.17	0.33	0.13	0.47	0.33
Total	100.38	100.23	100.85	99.43	98.48	100.36	99.18
Phase comp. (mol%)	An52(Or3)	An48(Or4)	An45(Or6)	En41Wo38	En37Wo33	En36Wo36	En35Wo31

Phase	Augite	Ilmenite				
Experiment (No.)	100D3-09	100D3-04	100D3-03	100D3-06	100D3-07	100D3-09
Temperature (°C)	940	1,040	1,000	980	960	940
SiO_2	49.94	0.08	0.25	0.23	0.25	0.46
TiO_2	0.60	52.73	50.67	51.24	51.23	50.98
Al_2O_3	1.54	0.32	0.22	0.19	0.20	0.24
FeO	22.58	41.22	43.45	44.14	43.96	44.15
MnO	0.54	0.49	0.60	0.68	0.60	0.62
MgO	10.86	4.13	2.41	2.00	2.08	1.58
CaO	13.55	0.12	0.58	0.48	0.50	0.38
Na_2O	0.15	0.04	0.03	0.02	0.04	0.02
K_2O	0.05	0.03	0.05	0.02	0.08	0.10
P_2O_5	0.23	0.00	0.02	0.02	0.07	0.01
Total	100.03	99.16	98.28	99.02	99.00	98.53
Phase comp. (mol%)	En33Wo28	Ilm98Hem2	Ilm97Hem3	Ilm97Hem3	Ilm97Hem3	Ilm98Hem2
Phase	Apatite				Pigeonite	
Experiment	100D3-03	100D3-06	100D3-07	100D3-09	100D3-09	
Temperature (°C)	1,000	980	960	940	940	
SiO_2	0.43	0.76	1.63	1.73	49.93	
TiO_2	0.05	0.12	0.07	0.08	0.51	
Al_2O_3	0.05	0.09	0.47	0.28	0.89	
FeO	1.18	1.10	1.26	1.19	30.05	
MnO	0.10	0.13	0.10	0.09	0.68	
MgO	0.27	0.20	0.26	0.20	12.75	
CaO	53.26	53.80	52.56	52.15	5.19	
Na_2O	0.03	0.03	0.03	0.05	0.04	
K_2O	0.08	0.07	0.04	0.20	0.04	
P_2O_5	40.47	41.19	39.79	40.01	0.11	
Total	95.92	97.50	96.21	95.98	100.20	
Phase comp. (mol%)	N/A	N/A	N/A	N/A	En37Wo13	

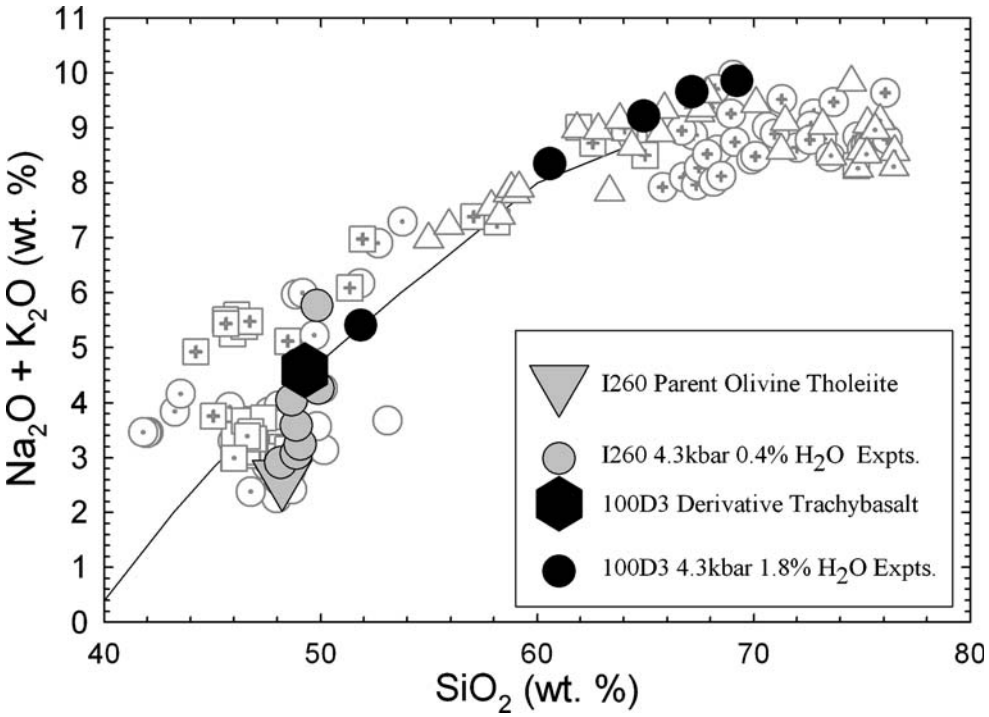

Fig. 7 Total alkalis vs. silica variation of residual liquid compositions (*black circles*) of experiments on 100D3 synthetic trachybasalt (*black hexagon*) at 4.3 kbar and 1.8 wt% bulk water content. Experimental residual liquids (*gray circles*) from I260 olivine tholeiite (*gray triangle*) at 4.3 kbar and 0.4 wt% bulk water content are also indicated in order to show the entire liquid line-of-descent from olivine tholeiite. Other symbols are as in Fig. 1

(940°C), pigeonite joins the crystallizing assemblage (Fig. 9).

Figure 10 shows the pyroxene and olivine compositions from the experiments on 100D3 as projected through QUILF (Andersen et al. 1993). The Fe-enrichment of the ferromagnesian mineral assemblages seen with decreasing temperature in the I260 experiments continues in these experiments as the residual melt evolves toward decreasing Mg#. The Fo content of the olivine decreases from Fo_{54} to Fo_{30} with falling temperature, while the En component of the augite decreases from En_{41} to En_{33}. The Wo content of the augites starts at the same level as the I260 experiments (Wo_{38}), but decreases significantly (Wo_{28}) as temperature decreases.

The relationships between the liquids, feldspars, and pyroxenes in these experiments in feldspar compositional space were obtained as described for the I260 experiments, and are shown in Fig. 11. The evolutionary paths of feldspars and the normative feldspar components of the liquid continue the trend initiated by experiments on I260. The anorthite component of the plagioclase decreases to An_{45} with decreasing temperature; the orthoclase component increases to Or_6. No alkali feldspar was detected in the experimental run products of any of these experiments; least squares calculations indicate that this phase was not overlooked during analysis.

The absence of alkali feldspar in the experimental assemblages is fully consistent with the ternary feldspar solvus. Figure 11 shows an isothermal feldspar solvus section at 4.3 kbar and 940°C (the lowest temperature experiment) calculated using SOLVCALC (Wen and Nekvasil 1994) and the ternary feldspar model of Lindsley and Nekvasil (1989). This diagram shows that the solidus, represented by the trend in plagioclase compositions, does not intersect the solvus, even at the lowest experimental temperature.

Discussion

Equilibrium crystallization of I260 at 4.3 kbar produced residual liquids that are similar to the mafic, intermediate and silicic rocks of the Laramie Anorthosite Complex and Snake River Plain. The mafic liquids produced do not show the strong Fe–Ti–P enrichment and silica-depletion of liquids produced experimentally during anhydrous crystallization at 9.3 kbar (Whitaker et al. 2003). Instead, the lower pressure residual liquids follow a subset of the natural basalts/gabbros of these suites (Fig. 8) that shows alkali enrichment at almost constant silica content.

Detailed comparison of the experimental residual liquids with the Cedar Butte and Craters of the Moon trends shows that these liquids fall slightly above the natural rock trend in Al_2O_3, and just below the trend in FeO_T. This could in part be caused by the high alumina and low iron contents of the starting material relative to many Snake River Plain basalts, but is more likely the result of the experimental conditions. Nekvasil et al. (2004) reported up to 10 rel. wt% error in determining the water contents of their experimental glasses because of irregularities in sample thickness. Since the same equipment and procedure was used in these analyses, similar errors may be expected. Slight increases in the bulk water

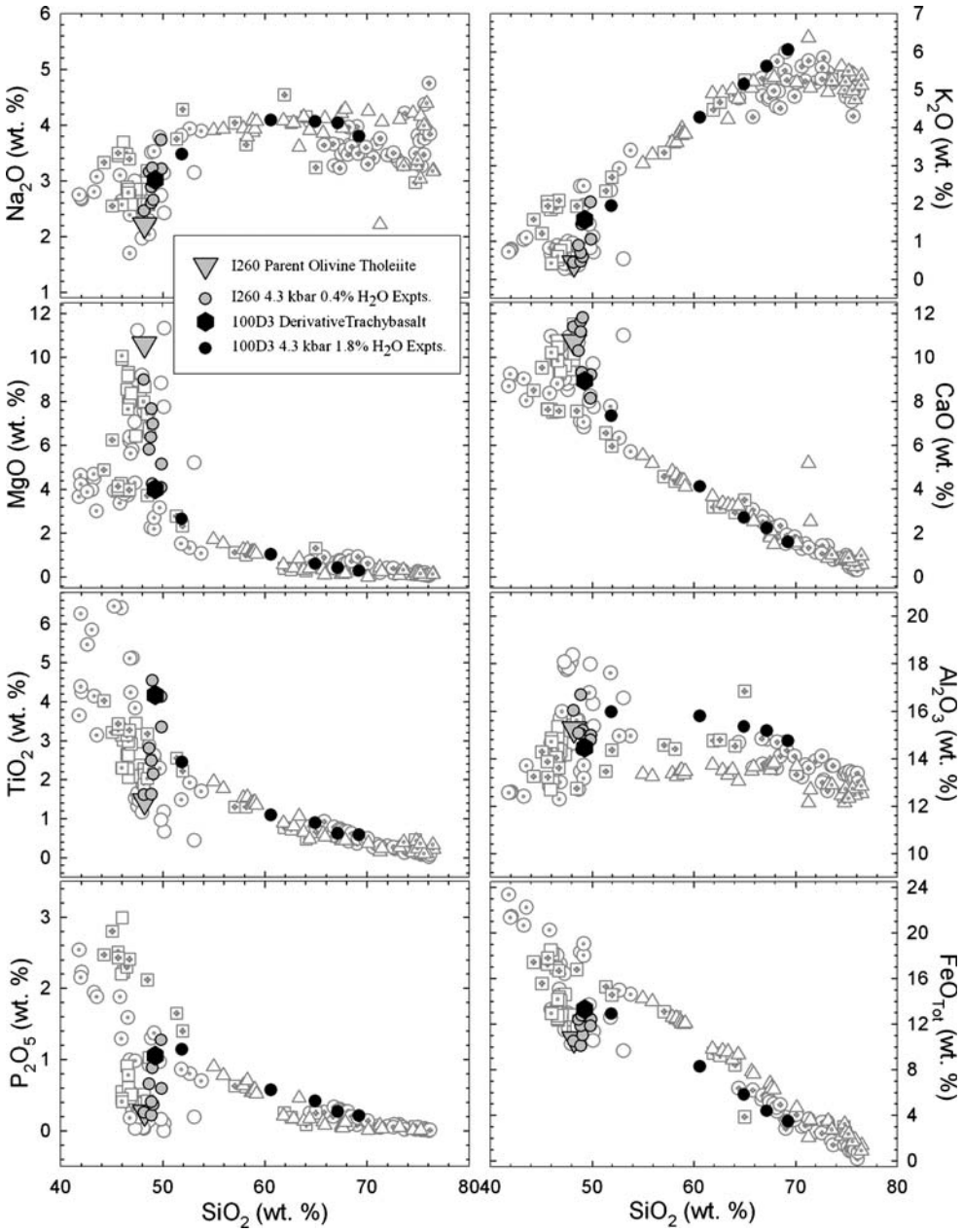

Fig. 8 Major element Harker variation diagrams of residual liquid compositions (*black circles*) of experiments on 100D3 (*black hexagon*) at 4.3 kbar and 1.8 wt% bulk water content. Residual liquids (*gray circles*) from I260 olivine tholeiite (*gray triangle*) at 4.3 kbar and 0.4 wt% bulk water content are also indicated in order to show the entire trend from olivine tholeiite. Other symbols are as in Fig. 1

content of the derivative starting material would have caused more plagioclase component to remain in the residual liquids, leading to elevated alumina contents. This may also account for the slightly low iron contents of the residual liquids, as the relative abundances of ferromagnesian minerals and Fe–Ti oxides in the assemblage would increase. What is important to note, however, is that despite a minor offset, the trajectories of the crystallization path and the natural rock trend are parallel.

Experimental verification of the possibility that equilibrium crystallization of tholeiite at mid-crustal levels can produce the intermediate magmas of the potassic silica-saturated appears inconsistent with their paucity in the Snake River Plain. However, intermediate rocks are not scarce in the massif anorthosite suites. This suggests that there may be physical impediments to ascent of the intermediate magmas to the surface. Since highly dense ferrobasalts have been found on the surface at the Craters of the Moon, density may not be the primary inhibiting variable. Instead, perhaps the high viscosity of intermediate magmas, with their high abundance of trachytic alkali feldspar, plays a major role.

Differentiation of the I260 olivine tholeiite parent material produces liquids that trend toward the evolved potassic rhyolitic/granitic compositions of the silica-saturated potassic series. However, the original tholeiite is ~96–97% crystalline (i.e. 80–86% crystallization of the 100D3 starting material, which was the result of ~80% crystallization of I260) by the time these liquids are produced. In the volcanic

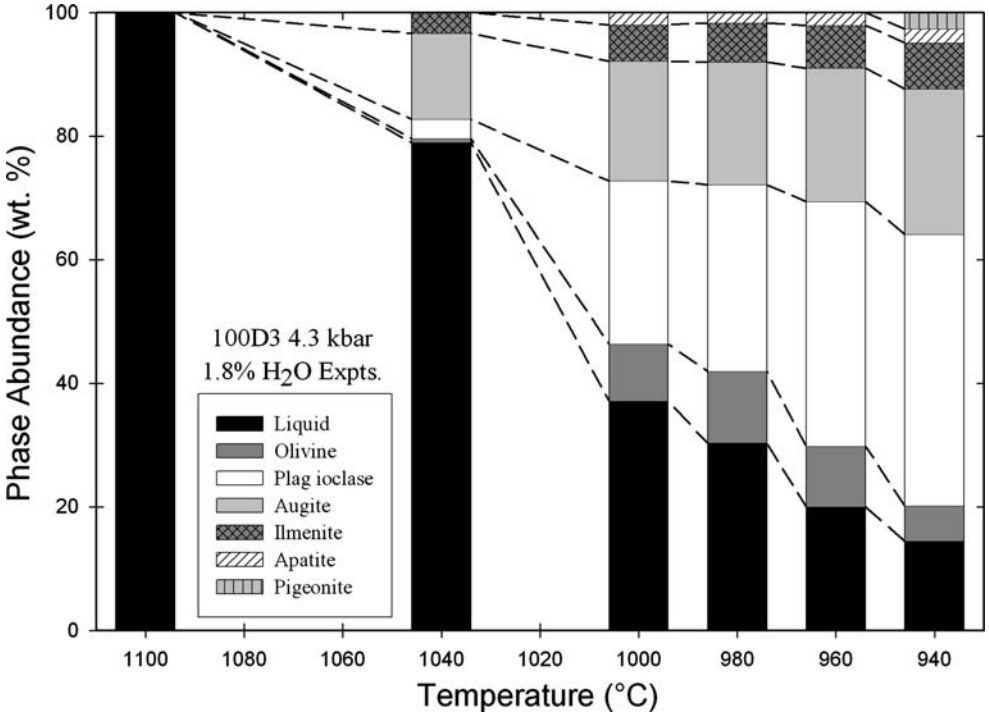

Fig. 9 Variation in phase abundances with temperature of experimental run products of 100D3 at 4.3 kbar and 1.8 wt% bulk water content

suites, the location of the voluminous crystalline residuum would be at depth, so volumetric relations exposed at the surface need not be a concern. Geophysical interpretations of the velocity and density structure of the Snake River Plain show a distinct mid-crustal high-density layer following the axis of the plain that extends from ~10–20 km depth within the crust (Peng and Humphreys 1998; Sparlin et al. 1982). Similar crustal structure has been found in the Fennoscandian region where plutonic rather than volcanic exposure is the norm. An anomalous high-velocity layer is found at a depth of ~15 km, underlying the Wiborg batholith (Luosto 1991; Luosto et al. 1990). These high-density layers could represent the cumulate residuum left behind following the ascent of residual liquids.

Depending upon the efficiency of liquid removal and the later-stage low-pressure crystallization history, the phenocryst assemblage in the rocks may show no evidence for the higher pressure history postulated here; the evidence for this history being preserved primarily in the bulk compositions of the rocks. For the olivine tholeiites of the Snake River Plain and the more mafic units of the Craters of the Moon suite, the absence of clinopyroxene phenocrysts speaks to a late-stage lower-pressure history since clinopyroxene plays a dominant role in the crystalline assemblages at higher pressure but crystallizes late at low pressure (e.g., Spulber and Rutherford 1983). In fact, thermobarometry calculations using pyroxenes of the more evolved members of the Cedar

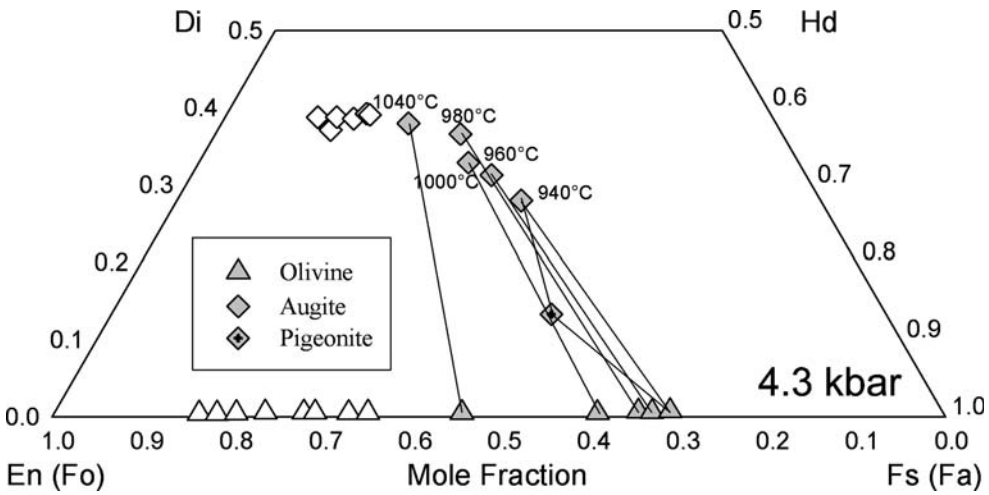

Fig. 10 QUILF projections of olivine and pyroxene compositions from experimental run products of 100D3 at 4.3 kbar and 1.8 wt% bulk water content (*gray symbols*). Tie-lines connect coexisting phases. Temperatures of experiments are indicated. QUILF projections of olivine and pyroxene compositions of experiments on I260 at 4.3 kbar and 0.4 wt% bulk water content are also indicated (*open symbols*) in order to show the entire trend

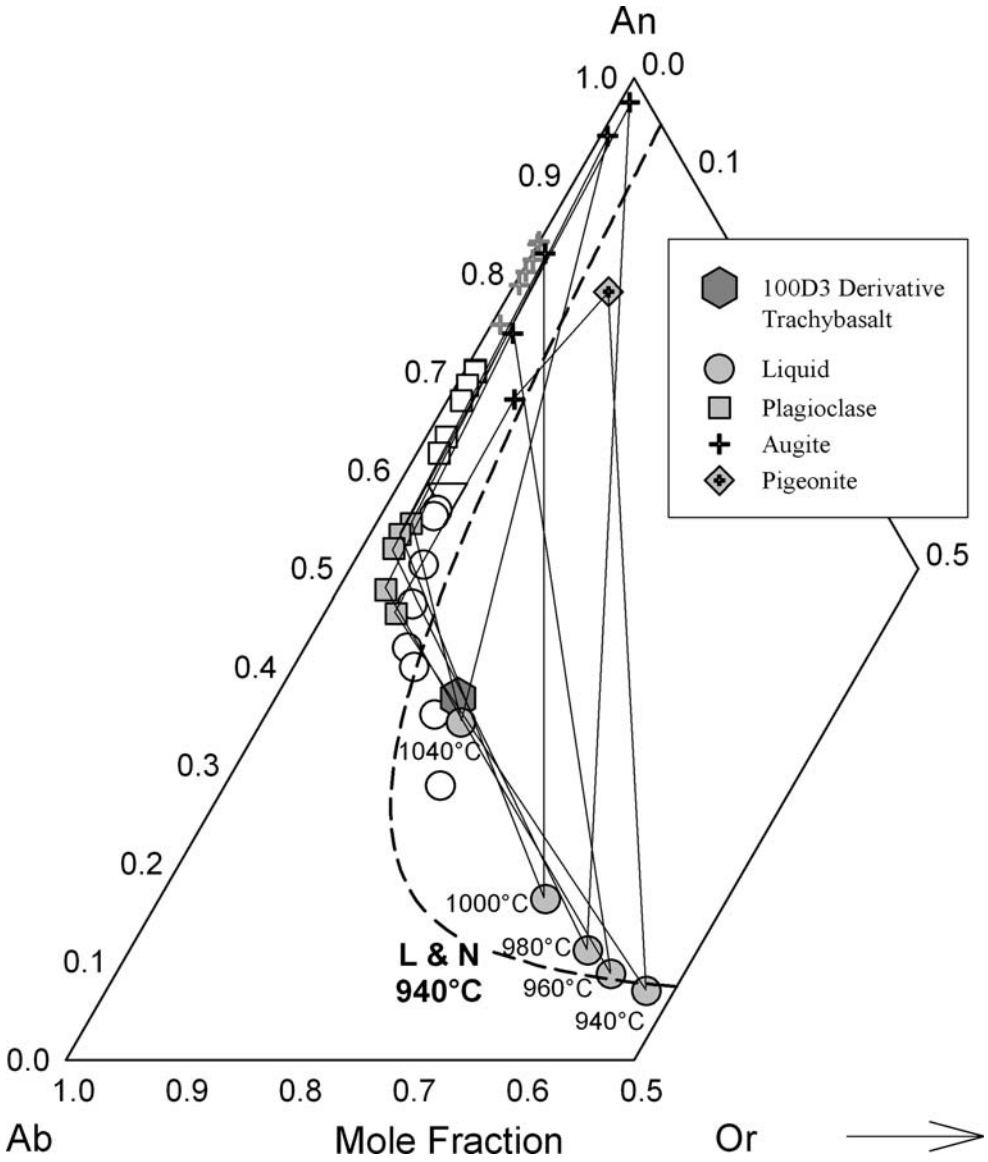

Fig. 11 Plagioclase compositions (*gray squares*) and molar normative feldspar constituents of glass (*gray circles*) and pyroxene (*black crosses*) of 100D3 (*gray hexagon*) experiments at 4.3 kbar and 1.8 wt% bulk water content. Tie-lines connect coexisting phases. Temperatures of these experiments are indicated. Experimental data from experiments on I260 (*open symbols*, *gray crosses*) are shown to demonstrate the entire trend from olivine tholeiite. The isothermal feldspar solvus section computed using the model of Lindsley and Nekvasil (1989) and the software of Wen and Nekvasil (1994) for 940°C and 4.3 kbar is shown by the *dashed curve*

Butte suite (McCurry et al. this issue) are consistent with a final low pressure crystallization stage.

Three primary problems remain when relating the experimental data to natural rocks in these silica-saturated potassic suites. First is the very high degree of crystallinity required to produce potassic rhyolite. This brings into question the viability of rhyolite production by separation of residual liquid. Second is the absence of alkali feldspar in the experimental assemblages. This mineral was not crystallized even in lower pressure experiments of DiFrancesco et al. (2003) and Whitaker et al. (personal communication), yet is abundant in the natural rocks. Finally, the experiments failed to produce the most evolved liquids of the natural suites: those marked by strong increases in Na and decreases in K at high silica contents. Each of these problems may be ameliorated by the presence of F.

The possible effects of fluorine

There is little evidence that these potassic rhyolites and granites were water-rich; however, there is evidence that evolved liquids of these potassic suites can contain significant amounts of fluorine. Topaz rhyolites have been reported in the western United States and Mexico (Christiansen et al. 1986), and subvolcanic equivalents of these rocks (ongonites) have been reported in Mongolia (Kovalenko 1973; Kovalenko et al. 1971). The elevated fluorine content of both the melt composition and a coexisting vapor phase in these rock types is indicated by the presence of both magmatic and hydrothermally precipitated fluorite and topaz. Potassic granites such as the Wiborg Rapakivi batholith in Finland commonly contain late-stage topaz-bearing granitic bodies (Haapala and Lukkari 2005). Some potassic granite samples (e.g., from the

Pikes Peak batholith in Colorado, Barker et al. 1975) exhibit elevated fluorine contents (up to 1 wt%), and many samples from the Sherman Batholith in Wyoming (Frost et al. 1999) contain F-bearing micas and amphiboles, as well as fluorite. The silicic volcanics associated with the Yellowstone hotspot and Snake River Plain, however, are generally much lower in F (Perkins and Nash 2002; Perkins et al. 1995); this may be caused by loss of fluorine during eruption and subsequent devitrification (Christiansen et al. 1986).

F interacts strongly with silicate melts (Lange 1994) by breaking framework bonds and forming Al–F (Kohn et al. 1991; Liu and Nekvasil 2001; Schaller et al. 1992; Zeng and Stebbins 2000) and Si–F complexes (Liu and Nekvasil 2002; Zeng and Stebbins 2000) in the melt. F suppresses the solidus temperature below that of the halogen-free water-saturated solidus, thereby allowing the production of greater volumetric abundances of these silicic compositions. In addition to the presence of F in the melt, crystal fractionation, rather than the equilibrium crystallization simulated here, would further contribute to the production of more voluminous amounts of residual silicic melt.

Suppression of the solidus temperature by F would allow the plagioclase solidus to evolve to the feldspar solvus and could lead to the crystallization of alkali feldspar. Furthermore, the documented preference of F for complexing with Na relative to K (Manning 1981) should decrease the activity of the albite component in the melt relative to the orthoclase component, thereby suppressing plagioclase crystallization relative to alkali feldspar. In combination, these effects may explain the apparent paradox posed by the internal consistency among experimental plagioclase, feldspathic components in the liquid, and experimental temperatures, yet the presence of alkali feldspar in the natural rocks. Fluorine-induced solidus temperature suppression and the suppression of plagioclase crystallization (that is, enhancement of its solubility) by F may also explain why high Na, low K high silica rhyolitic liquids were not produced experimentally. Enhancement of the solubility of the albite component in fluorinated melt will yield residual melts increasingly enriched in sodium relative to potassium as is characteristic of the most evolved rhyolites of these suites.

The experiments presented here have illustrated the possibility of producing potassic rhyolitic magma by equilibrium crystallization of typical continental olivine tholeiite at mid-crustal levels. Partial melting of basalt, however, is not precluded by these results. Discrimination between these two processes must be done on an individual suite basis by assessment of trace element systematics. Such analysis by McCurry et al. (1999; this issue) suggests that liquid differentiation may be the preferred mechanism for generating potassic rhyolitic liquids of Cedar Butte. This result may be applicable to other potassic rhyolites of the Snake River Plain, other bimodal intra-plate suites, and the potassic granites of the anorthosite complexes and rapakivi granite provinces.

The experimental results presented here provide a foundation upon which to build and assess models for assimilation, magma mixing, and magma ascent and distribution. Further experimentation on fluorinated systems is needed for insight into possible co-genetic relationships among the most highly evolved rocks in these potassic silica-saturated suites.

Acknowledgment This paper is dedicated to Prof. Ilmari Haapala with great appreciation for his many years of outstanding work on the potassic granites of Fennoscandia. The authors would like to thank S. A. Morse, C. W. Mandeville, and E. H. Christiansen for insightful and constructive reviews of this manuscript. The authors acknowledge the financial support of NSF grant EAR 0003443 to DHL and HN, and EG&G Idaho contract C84-110421 to MM.

References

Andersen DJ, Lindsley DH, Davidson PM (1993) QUILF—a Pascal program to assess equilibria among Fe–Mg–Mn–Ti oxides, pyroxenes, olivine, and quartz. Comput Geosci 19:1333–1350

Anderson JL (1983) Proterozoic anorogenic granite plutonism of North America. In: Medaris LG Jr, Byers CW, Mickelson DM, Shanks WC (eds) Geol Soc Am Memoir 161:133–154

Barker F, Wones DR, Sharp WN, Desborough GA (1975) Pikes Peak Batholith, Colorado Front Range, and model for origin of "gabbro–anorthosite–syenite–potassic granite" suite. Precambrian Res 2:97–160

Carr MJ (2002) IgPet for Windows. Terra Softa, Somerset, NJ

Christiansen EH, McCurry M (2007) Contrasting origins of Cenozoic silicic volcanic rocks from the Western Cordillera of the United States. Bull Volcanol (this issue)

Christiansen EH, Sheridan MF, Burt DM (1986) The geology and geochemistry of Cenozoic topaz rhyolites from the Western United States. Geol Soc Am Special Paper 205:82

DiFrancesco NJ, Whitaker ML, Nekvasil H, Lindsley DH (2003) A road to rhyolite: fractional crystallization experiments on a continental olivine tholeiite. Geol Soc Am 35:631

Dixon JE, Stolper EM, Holloway JR (1995) An experimental study of water and carbon dioxide solubilities in mid-ocean ridge basaltic liquids. Part 1: calibration and solubility models. J Petrol 36:1607–1631

Emslie RF (1978) Anorthosite massifs, rapakivi granites, and Late Proterozoic rifting of North America. Precambrian Res 7:61–98

Emslie RF (1991) Granitoids of rapakivi granite–anorthosite and related associations. Precambrian Res 51:173–192

Frost CD, Frost BR (1997) Reduced rapakivi-type granites: the tholeiite connection. Geology 25:647–650

Frost BR, Frost CD, Lindsley DH, Scoates JS, Mitchell JN (1993) The Laramie Anorthosite Complex and Sherman Batholith: geology, evolution, and theories of origin. In: Geology of Wyoming. Geol Surv Wyoming Memoir 5:118–161

Frost CD, Frost BR, Chamberlain KR, Edwards BR (1999) Petrogenesis of the 1.43 Ga Sherman batholith, SE Wyoming, USA: a reduced, rapakivi-type anorogenic granite. J Petrol 40:1771–1802

Haapala I, Lukkari S (2005) Petrological and geochemical evolution of the Kymi stock, a topaz granite cupola within the Wiborg rapakivi batholith, Finland. Lithos 80:347–362

Haapala I, Ramo OT (1990) Petrogenesis of the Proterozoic rapakivi granites of Finland. In: Stein HJ, Hannah JL (ed) Geol Soc Am Special Paper 246:275–286

Hunter RH, Sparks RSJ (1987) The differentiation of the Skaergaard intrusion. Contrib Mineral Petrol 95:451–461

Irvine TN, Baragar WRA (1971) Guide to chemical classification of common volcanic rocks. Can J Earth Sci 8:523–548

Kohn SC, Dupree R, Mortuza MG, Henderson CMB (1991) NMR evidence for five- and six-coordinated aluminum fluoride complexes in F-bearing aluminosilicate glasses. Am Mineral 76:309–312

Kovalenko VI (1973) Distribution of fluorine in a topaz-bearing quartz keratophyre dike (ongonite) and solubility of fluorine in granitic melts. Geochem Int 10:41–49

Kovalenko VI, Kuzmin MI, Antipin VS, Petrov LL (1971) Topaz-bearing quartz keratophyre (ongonite)—a new variety of subvolcanic veined magmatic rocks. Dokl Akad Nauk SSSR 199:430

Kuntz MA, Covington HR, Schorr LJ (1992) An overview of basaltic volcanism of the eastern Snake River plain, Idaho. In: Link PK, Kuntz MA, Platt LB (eds) Geol Soc Am Memoir 179:227–267

Lange RA (1994) The effect of H2O, CO2 and F on the density and viscosity of silicate melts. In: Carroll MR, Holloway JR (eds) Rev Miner 30:331–369

Leeman WP (1982) Evolved and hybrid lavas from the Snake River Plain, Idaho. In: Bonnichsen B, Breckenridge RM (eds) Idaho Bureau of Mines and Geology Bulletin 26:193–202

Leeman WP (1982) Rhyolites of the Snake River Plain–Yellowstone Plateau province, Idaho and Wyoming; a summary of petrogenetic models. In: Bonnichsen B, Breckenridge RM (eds) Idaho Bureau of Mines and Geology Bulletin 26:203–212

Leeman WP, Vitaliano CJ, Prinz M (1976) Evolved lavas from the Snake River Plain—craters of the Moon National Monument, Idaho. Contrib Mineral Petrol 56:35–60

Lindsley DH, Andersen DJ (1983) A two-pyroxene thermometer. J Geophys Res B 88:A887–A906

Lindsley DH, Nekvasil H (1989) A ternary feldspar model for all reasons. EOS Trans Am Geophys Union 70:506

Litvin VY (2002) Application of fractional crystallization to the origin of continental tholeiitic suites. MS thesis, State University of New York at Stony Brook, Stony Brook, p 138

Liu Y, Nekvasil H (2001) Ab initio studies of possible fluorine-bearing four- and fivefold coordinated Al species in aluminosilicate glasses. Am Mineral 86:491–497

Liu Y, Nekvasil H (2002) Si–F bonding in aluminosilicate glasses: inferences from ab initio NMR calculations. Am Mineral 87:339–346

Luosto U (1991) Crustal structures of Eastern Fennoscandia. Tectonophysics 189:19–27

Luosto U, Tiira T, Korhonen H, Azbel I, Burmin V, Buyanov A, Kosminskaya I, Ionkis V, Sharov N (1990) Crust and upper mantle structure along the DSS Baltic profile in SE Finland. Geophys J Int 101:89–110

Mandeville CW, Webster JD, Rutherford MJ, Taylor BE, Timbal A, Faure K (2002) Determination of molar absorptivities for infrared absorption bands of H2O in andesitic glasses. Am Mineral 87:813–821

Manning DAC (1981) An experimental study of the effects of F on the crystallization of granitic melts. J Geol Soc Lond 138:213–214

McCurry M, Hackett WR, Hayden K (1999) Cedar Butte and cogenetic Quaternary rhyolite domes of the Eastern Snake River Plain. In: Hughes SS, Thackray GD (ed) Guidebook to the Geology of Eastern Idaho. Idaho Museum of National History, pp 169–179

McCurry M, Hayden KP, Morse LH, Mertzman S (2007) Genesis of post-hotspot A-type rhyolite of the Eastern Snake River Plain volcanic field by extreme fractional crystallization of olivine tholeiite. Bull Volcanol (this issue)

Mitchell JN, Scoates JS, Frost CD (1995) High–Al gabbros in the Laramie Anorthosite Complex, Wyoming—implications for the composition of melts parental to Proterozoic anorthosite. Contrib Mineral Petrol 119:166–180

Mitchell JN, Scoates JS, Frost CD, Kolker A (1996) The geochemical evolution of anorthosite residual magmas in the Laramie Anorthosite Complex, Wyoming. J Petrol 37:637–660

Nekvasil H (1998) Massif anorthosites, anorogenic granites and rift-related tholeiites and ferrobasalts; is there a connection? Geol Soc Am 30:236

Nekvasil H, Simon A, Lindsley DH (2000) Crystal fractionation and the evolution of intra-plate hy-normative igneous suites: insights from their feldspars. J Petrol 41:1743–1757

Nekvasil H, Lindsley DH, Whitaker ML, Filiberto J, DiFrancesco NJ, Rossier L, Horn J (2003) Tholeiites, anorthosites, potassic granites, sodic trachytes, and tephriphonolites: is there a link? Geol Soc Am 35:395

Nekvasil H, Dondolini A, Horn J, Filiberto J, Long H, Lindsley DH (2004) The origin and evolution of silica-saturated alkalic suites: an experimental study. J Petrol 45:693–721

Newton RC, Charlu TV, Kleppa OJ (1974) Calorimetric investigation of stability of anhydrous magnesium cordierite with application to granulite facies metamorphism. Contrib Mineral Petrol 44:295–311

Peng XH, Humphreys ED (1998) Crustal velocity structure across the eastern Snake River Plain and the Yellowstone swell. J Geophys Res 103:7171–7186

Perkins ME, Nash BP (2002) Explosive silicic volcanism of the Yellowstone hotspot: the ash fall tuff record. Geol Soc Am Bull 114:367–381

Perkins ME, Nash WP, Brown FH, Fleck RJ (1995) Fallout tuffs of Trapper Creek, Idaho—a record of Miocene explosive volcanism in the Snake River Plain volcanic province. Geol Soc Am Bull 107:1484–1506

Rossier L, Lindsley DH, Nekvasil H, Scoates JS (2001) The origin of potassic granite: results of fractional crystallization experiments on a high-Al olivine gabbro from the Laramie Anorthosite Complex, Wyoming. Geol Soc Am 33:87

Schaller T, Dingwell DB, Keppler H, Knoller W, Merwin L, Sebald A (1992) Fluorine in silicate glasses: a multinuclear nuclear magnetic resonance study. Geochim Cosmochim Acta 56:701–707

Scoates JS, Frost CD, Mitchell JN, Lindsley DH, Frost BR (1996) Residual-liquid origin for a monzonitic intrusion in a mid-Proterozoic anorthosite complex: the Sybille intrusion, Laramie Anorthosite Complex, Wyoming. Geol Soc Am Bull 108:1357–1371

Scoates JS, Lindsley DH, van der Kolk D, Anderson K (1999) Fractional crystallization experiments on a candidate parental magma to anorthosite. EOS Trans Am Geophys Union 80: F1096

Sparlin MA, Braile LW, Smith RB (1982) Crustal structure of the Eastern Snake River Plain determined from ray trace modeling of seismic refraction data. J Geophys Res 87:2619–2633

Spulber SD, Rutherford MJ (1983) The origin of rhyolite and plagiogranite in oceanic crust— n experimental study. J Petrol 24:1–25

Stout MZ, Nicholls J (1977) Mineralogy and petrology of Quaternary lavas from the Snake River Plain, Idaho. Can J Earth Sci 14:2140–2156

Stout MZ, Nicholls J, Kuntz MA (1994) Petrological and mineralogical variations in 2500–2000 yr B.P. lava flows, Craters of the Moon lava field, Idaho. J Petrol 35:1681–1715

Thompson RN (1975) Primary basalts and magma genesis II. Snake River Plain, Idaho, USA. Contrib Mineral Petrol 52:213–232

Vorma A (1976) On the petrochemistry of rapakivi granites with special reference to the Laitila Massif, southwestern Finland. Geol Surv Finland Bull 285:98

Wen S, Nekvasil H (1994) Solvcalc: an interactive graphics program package for calculating the ternary feldspar solvus and for two-feldspar geothermometry. Comput Geosci 20:1025–1040

Whitaker ML, DiFrancesco NJ, Lindsley DH, Nekvasil H (2003) Can fractionation of an olivine tholeiite give rise to ferrodiorites, ferrobasalts, and anorthosites? Geol Soc Am 35:631

Whitaker ML, Nekvasil H, Lindsley DH (2004) Can fractionation of an olivine tholeiite give rise to potassic rhyolites? Geol Soc Am 36:25

Zeng Q, Stebbins JF (2000) Fluoride sites in aluminosilicate glasses: high-resolution 19F NMR results. Am Mineral 85:863–867